Available online at www.sciencedirect.com

ScienceDirect

Mendeleev Commun., 2023, **33**, 866–868

Mendeleev Communications

Formation of a single-ion magnet in the lanthanum calcium silicate apatite structure by the cobalt oxide doping

Timur Z. Sharifullin,[a] Alexander V. Vasiliev,[a] Artem A. Eliseev,[a] Andrei A. Eliseev,[a] Sebastian Bette,[b] Robert E. Dinnebier,[b] Reinhard K. Kremer[b] and Pavel E. Kazin*[a]

[a] *Department of Chemistry, M. V. Lomonosov Moscow State University, 119991 Moscow, Russian Federation. E-mail: kazin@inorg.chem.msu.ru*

[b] *Max Planck Institute for Solid State Research, 70569 Stuttgart, Germany*

DOI: 10.1016/j.mencom.2023.10.043

A small amount of cobalt was incorporated into the lanthanum calcium silicate apatite structure by annealing at 1500 °C in argon. The compound exhibits easy-axis magnetic anisotropy with a zero-field splitting parameter 2*D* of −60 cm^{-1} and field-induced slow relaxation of magnetization with a remagnetization energy barrier of 58–63 cm^{-1}. Thereby, for the first time, a cobalt-based single-ion magnet was created in silicate.

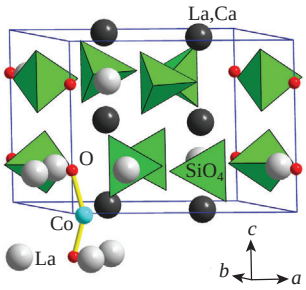

Keywords: silicate, apatite, single molecule magnet, single-ion magnet, crystal structure, magnetic properties.

Single-molecule magnets (SMMs) are atomic scale permanent magnets comprising an exchange-coupled group of open-shell transition metal ions in a polynuclear complex or a single transition metal ion in a mononuclear complex. The latter is also called a single-ion magnet (SIM). In order to invert the SMM magnetization, it is required to overcome the energy barrier (U_{eff}), which arises due to the high magnetic anisotropy of the molecule. The field of SMM research, which began with the discovery of the manganese complex in 1993,[1] has grown rapidly as such materials have proven to be promising candidates for ultra-high-density memory devices, molecular electronics, spintronics and quantum computing.[2–9] Most known SMMs are metal complexes with organic ligands. Along with this, SIMs can be created by incorporating transition metal cations into extended inorganic solids, but the number of such systems is much smaller.[10] Among the *d*-element cations, Co^{2+} turned out to be the most promising for SIM centers due to its pronounced magnetic anisotropy.[11,12] With respect to inorganic solids, Co^{2+} has been shown to enter the crystal structure of alkaline-earth-metal phosphate apatites, forming bent $[O–Co–O]^{2-}$ units in trigonal channels.[13–19] Such compounds exhibit the slow relaxation of magnetization inherent in SIMs. The U_{eff} value is 59 and 65 cm^{-1} in Sr and Ca apatites, respectively,[14–17] and abruptly reaches 387 cm^{-1} in Ba apatite.[18,19] Considering that the record value for cobalt-based SMMs is only 450 cm^{-1},[20] the apatite matrix seems to be very promising for hosting SIM centers with high U_{eff}. In this work, we have investigated for the first time the possibility of forming Co-based SIM centers in the structure of a silicate apatite.

Samples of the nominal composition $La_7Ca_3(SiO_4)_6Co_x(OH_{1-y})_2$, where $x = 0.07$ (**1**) or 0.4 (**2**) and $y < 1$, were prepared by a solid-state reaction with final treatment at a temperature of 1500 °C in an argon flow. The samples were studied by high-precision powder X-ray diffraction (XRD), scanning electron microscopy with elemental (EDX) analysis, Raman spectroscopy, and ac and dc magnetometry (for more experimental details, see Online Supplementary Materials).

According to XRD data (Figures S1 and S2, see Online Supplementary Materials), the samples are dominated by the apatite phase with small impurities of Ca_3SiO_5 in sample **1** and Ca_2SiO_4 and La_2CoO_4 in sample **2**. The polycrystalline samples consist of elongated grains with a typical size of 5–20 μm. EDX analysis of the areas within the grains shows an enrichment in La at the expense of Ca, so that the ratio of the elements La/Ca/Si shifts from the nominal 7 : 3 : 6 to 7.9 : 2.1 : 6, which is the same in both samples (with a standard deviation of 0.2). This is consistent with the presence of calcium silicate impurities and indicates the instability of OH^- in the silicate apatite under the conditions of preparation, which leads to the simultaneous replacement of OH^- by O^{2-} and Ca^{2+} by La^{3+}. Co is found in grains in a small amount, corresponding to x of 0.02(1) and 0.06(1) for samples **1** and **2**, respectively. This finding implies a very limited solubility of Co in the silicate apatite. The remainder of Co appears to be contained in the impurity phases.

The crystal structures were refined by the Rietveld method in the space group $P6_3/m$ using the Jana2006 program.[21] A fragment of the apatite crystal structure is depicted in Figure 1. Structural

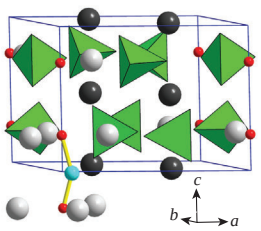

Figure 1 Projection of a fragment of the crystal structure of silicate apatite **1** under normal conditions, showing the unit cell and part of the trigonal channel on the left front edge. Large gray balls are M1 ($La_{0.51}Ca_{0.49}$), large dark gray balls are M2 ($La_{0.93}Ca_{0.07}$), green tetrahedra are SiO_4 groups, small red balls are oxygen atoms in the trigonal channels, and a medium-sized blue ball is a Co atom (proposed location according to ref. 16).

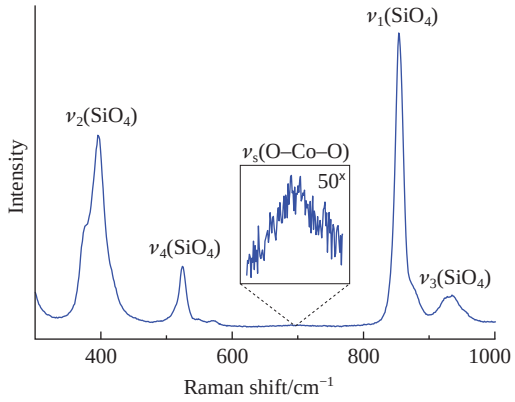

Figure 2 Raman spectrum of silicate apatite **1** measured at room temperature.

parameters are listed in Tables S1–S4. Structural features are close to those published for $La_8Ca_2(SiO_4)_6O_2$.[22] The La and Ca cations occupying Wyckoff position 6*h* (M2, c. n. 7) form the 'walls' of trigonal channels filled with small anions, O^{2-} and OH^-. The La and Ca cations at the Wyckoff position 4*f* (M1, c. n. 6 + 3) form linear columns along the *c*-axis. M2 is almost completely occupied by La, while M1 is equally occupied by La and Ca. The refined quantity of La and Ca corresponds to the La/Ca ratio of 7.7 : 2.3 for sample **1** and 7.8 : 2.2 for sample **2**, which is in accord with the data obtained by the EDX analysis. In Co-doped phosphate apatites, Co is located in the trigonal channel near the position (0, 0, 0).[13,14,16,18] However, in the structure of silicate apatites **1** and **2**, we cannot localize Co atoms from the Rietveld refinements, apparently because of the low content. Nevertheless, the difference Fourier mapping reveals a weak maximum (+0.2e) of the electron density near the position (0.05, 0.05, 0.01), where Co atoms were also located in the phosphate apatite $Ca_{10}(PO_4)_6[(CoO_2)_{0.4}(OH)_{1.2}]$.[16] This observation suggests that the Co^{2+} cations in silicate apatites **1** and **2** are located in the trigonal channels.

The Raman spectra of silicate apatite **1** (Figure 2), along with strong SiO_4^{4-} vibration bands characteristic of silicate apatite,[23] show a weak band at 700 cm^{-1}. It has been reported that the $[O–Co–O]^{2-}$ group of atoms in the calcium phosphate apatite exhibits a characteristic band of symmetric stretching vibration at 713 cm^{-1}.[16] Accordingly, we also attribute the weak band in the spectrum of silicate apatite **1** to this group of atoms.

For silicate apatites **1** and **2**, the ac susceptibilities were measured down to T = 2 K. The samples show paramagnetic behavior of a Curie–Weiss type. Slow relaxation of the magnetization is observed below 10 K and only when a dc magnetic field is applied. The ac susceptibilities χ' and χ'' measured as a function of the ac field frequency (f) in a dc field of 4 kOe are shown in Figures S3 and S4. At temperatures from 2 to 8 K, a maximum of $\chi''(f)$ is observed for both samples, indicating the presence of a slow relaxation of magnetization characteristic of SIMs. $\chi'(f)$ and $\chi''(f)$ were fitted to the generalized Debye model[24] [equations (S1) and (S2), see Online Supplementary Materials] to obtain the relaxation time (τ), equilibrium (χ_0) and adiabatic (χ_s) susceptibilities, and the width of the relaxation time distribution (α).

At T = 2 K, the fitted values of χ_0 are 0.0204 and 0.0400 cm^3 per mole of apatite for samples **1** and **2**, respectively. Physically, χ_0 is equal to the differential dc susceptibility at an applied dc field. It is expected that at T = 2 K χ_0 is mainly determined by the lowest energy doublet of Co^{2+} formed in the axial crystal field. Using the PHI software,[25] for the ground doublet with $M_S = \pm 3/2$ (expected for Co^{2+} with easy-axis anisotropy) and the g-factors found for the Co-doped calcium phosphate apatite,[14] we estimate the theoretical value for the differential susceptibility to be 0.709 cm^3 per mole of Co. Taking this into account, the experimental values of χ_0 correspond to the content of paramagnetic cobalt ions x = 0.029 and 0.056 per formula unit for samples **1** and **2**, respectively. These values agree well with the Co concentration found in the apatite phase by EDX analysis. Apparently, the rest of Co does not make a noticeable contribution to the magnetic susceptibility. It can be represented by antiferromagnetically coupled (*e.g.*, Co^{2+} in the La_2CoO_4 impurity) or diamagnetic (*e.g.*, low-spin Co^{3+}) species.

Figure 3 displays the relaxation times in the form of Arrhenius plots of ln(τ) *vs.* 1/T. The temperature dependence of τ is usually analyzed using equation (1):

$$\tau^{-1} = \tau_{QTM}^{-1} + BT + CT^n + \tau_0^{-1} \exp(-U_{eff}/k_BT), \quad (1)$$

which takes into account several relaxation mechanisms. The term τ_{QTM}^{-1} considers quantum tunneling of the magnetization (QTM), and the following terms describe direct relaxation, Raman relaxation and thermally activated Orbach relaxation processes, respectively.[7] The QTM contribution was set to zero because the dependence of ln(τ) on 1/T does not show asymptotic saturation at low temperatures. The fitted parameters are as follows: B = 16.4(5) s^{-1} K^{-1}, C = 0.02(2) s^{-1} K^{-n}, n = 5.0(7), τ_0 = 1.3(5) × 10^{-9} s and U_{eff} = 63(2) cm^{-1} for sample **2** and B = 23.7(9) s^{-1} K^{-1}, C = 0.011(4) s^{-1} K^{-n}, n = 5.0, τ_0 = 4.0(2) × 10^{-9} s and U_{eff} = = 58(3) cm^{-1} for sample **1**. The value of n for sample **1** was set to the value estimated for sample **2** to avoid overparametrization. The determined values of U_{eff} coincide within one standard deviation, which indicates the absence of a noticeable effect of the Co concentration on the energy barrier. In addition, the value of U_{eff} is close to the values found for calcium and strontium phosphate apatites doped with Co.[14–17] This suggests that the SIM unit in the silicate and phosphate apatites is the same, namely, the bent $[O–Co–O]^{2-}$ group located in the trigonal channel. Compared to the phosphate apatite, the parameter τ_0 takes values approximately an order of magnitude higher. The main difference is that $[O–Co–O]^{2-}$ is surrounded by triply charged La cations in the silicate and doubly charged cations in the phosphates. This changeover may induce a decrease in the partial charge on the oxygen atoms in the SIM unit of the first compound and thus reduce the crystal field strength, which allows an increase in the contribution of angular momentum to the electronic states of the SIM.

The low-temperature magnetization and the temperature dependence of the magnetic susceptibility–temperature product for sample **1** are shown in Figure 4. The first plot was modeled using the PHI software. Zero-field splitting in an axial crystal field was considered with the ground doublet $M_S = \pm 3/2$. g-Factors were taken as they were determined for the Co-doped calcium phosphate apatite ($g_x = g_y$ = 2.1, g_z = 2.4).[16] Very good agreement was achieved for 2D = −60 cm^{-1} and for the fraction of paramagnetic cobalt equal to 0.40. Taking into account the derived parameters, the dependence of χT on T was calculated. As can be seen from the inset to Figure 4, it reproduces the experimental data reasonably well. The absolute value of 2D

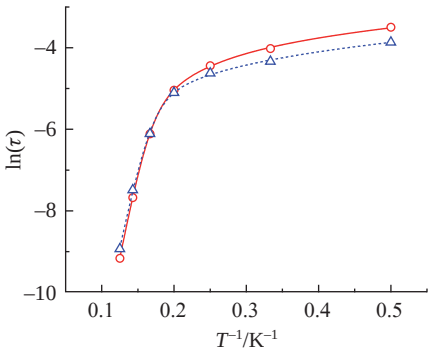

Figure 3 Temperature (T) dependence of the magnetization relaxation time τ(s) in silicate apatites **1** (blue triangles) and **2** (red circles). The dashed and solid lines are fittings to equation (1) with the parameters specified in the text.

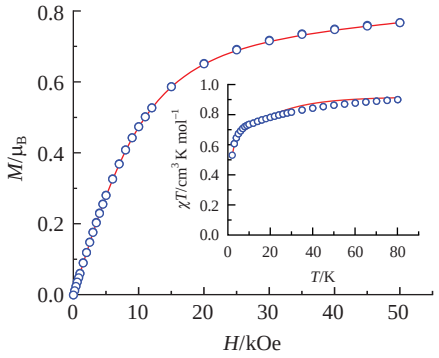

Figure 4 Field (*H)* dependence of the magnetization (*M*) of sample **1** at $T = 2$ K per mole of Co. Inset: temperature (*T*) dependence of the susceptibility–temperature product (χT) of sample **1** at $H = 10$ kOe per mole of Co. Circles represent experimental data, while lines are from modeling.

denotes the difference between the ground, $M_S = \pm 3/2$, and the first exited, $M_S = \pm 1/2$, Kramers doublets. The derived value matches well with the experimental values of U_{eff} determined from the magnetization relaxation data. A similar agreement between 2*D* and U_{eff} has been previously demonstrated for Co-doped Ca-phosphate hydroxyapatite.[16] Our results imply that magnetization reversal occurs by the Orbach process *via* the first exited electronic doublet.

In summary, Co can be introduced into the structure of La–Ca silicate apatite in a small amount, not exceeding a few mole percent. The results of the crystal structure refinement in combination with Raman spectroscopy indicate that Co^{2+} cations enter the trigonal channels of apatite, forming $[O–Co–O]^{2–}$ groups of atoms. Magnetic measurements confirm the slow relaxation of magnetization with characteristic parameters close to those found earlier for $[O–Co–O]^{2–}$ embedded in Ca- and Sr-phosphate apatites. Thus, SIM based on $[O–Co–O]^{2–}$ was first created in a solid apatite-type matrix, different from phosphate one, and demonstrated that the SIM parameters weakly depend on the nature of the matrix.

This work was supported by the Russian Science Foundation (grant no. 21-13-00238). The authors are grateful to E. Brücher for help with magnetic measurements and C. Stefani for powder XRD measurements.

Online Supplementary Materials

Supplementary data associated with this article can be found in the online version at doi: 10.1016/j.mencom.2023.10.043.

References

1 R. Sessoli, D. Gatteschi, A. Caneschi and M. A. Novak, *Nature*, 1993, **365**, 141.
2 M. Mannini, F. Pineider, P. Sainctavit, C. Danieli, E. Otero, C. Sciancalepore, A. M. Talarico, M.-A. Arrio, A. Cornia, D. Gatteschi and R. Sessoli, *Nat. Mater.*, 2009, **8**, 194.
3 S. Kyatskaya, J. R. Galán Mascarós, L. Bogani, F. Hennrich, M. Kappes, W. Wernsdorfer and M. Ruben, *J. Am. Chem. Soc.*, 2009, **131**, 15143.
4 C. Godfrin, S. Thiele, A. Ferhat, S. Klyatskaya, M. Ruben, W. Wernsdorfer and F. Balestro, *ACS Nano*, 2017, **11**, 3984.
5 C. A. P. Goodwin, F. Ortu, D. Reta, N. F. Chilton and D. P. Mills, *Nature*, 2017, **548**, 439.
6 F.-S. Guo, B. M. Day, Y.-C. Chen, M.-L. Tong, A. Mansikkamäki and R. A. Layfield, *Angew. Chem., Int. Ed.*, 2017, **56**, 11445.
7 A. Zabala-Lekuona, J. M. Seco and E. Colacio, *Coord. Chem. Rev.*, 2021, **441**, 213984.
8 E. Coronado, *Nat. Rev. Mater.*, 2020, **5**, 87.
9 Z. Zhu and J. Tang, *Chem. Soc. Rev.*, 2022, **51**, 9469.
10 M. A. Zykin, P. E. Kazin and M. Jansen, *Chem. – Eur. J.*, 2020, **26**, 8834.
11 P. K. Sahu, R. Kharel, S. Shome, S. Goswami and S. Konar, *Coord. Chem. Rev.*, 2023, **475**, 214871.
12 D. S. Yambulatov, S. A. Nikolaevskii, M. A. Shmelev, K. A. Babeshkin, D. V. Korchagin, N. N. Efimov, A. S. Goloveshkin, P. A. Petrov, M. A. Kiskin, M. N. Sokolov and I. L. Eremenko, *Mendeleev Commun.*, 2021, **31**, 624.
13 P. E. Kazin, O. R. Gazizova, A. S. Karpov, M. Jansen and Y. D. Tretyakov, *Solid State Sci.*, 2007, **9**, 82.
14 P. E. Kazin, M. A. Zykin, W. Schnelle, Y. V. Zubavichus, K. A. Babeshkin, V. A. Tafeenko, C. Felser and M. Jansen, *Inorg. Chem.*, 2017, **56**, 1232.
15 M. A. Zykin, A. A. Eliseev, A. V. Vasiliev, R. K. Kremer, R. E. Dinnebier, M. Jansen and P. E. Kazin, *Eur. J. Inorg. Chem.*, 2019, 4677.
16 M. A. Zykin, K. A. Babeshkin, O. V. Magdysyuk, E. O. Anokhin, W. Schnelle, C. Felser, M. Jansen and P. E. Kazin, *Inorg. Chem.*, 2017, **56**, 14077.
17 M. A. Zykin, E. O. Anokhin and P. E. Kazin, *Russ. Chem. Bull.*, 2019, **68**, 751.
18 P. E. Kazin, M. A. Zykin, L. A. Trusov, A. A. Eliseev, O. V. Magdysyuk, R. E. Dinnebier, R. K. Kremer, C. Felser and M. Jansen, *Chem. Commun.*, 2017, **53**, 5416.
19 M. A. Zykin, A. A. Eliseev, M. A. Pogosova, L. A. Trusov, W. Schnelle, C. Felser, M. Jansen and P. E. Kazin, *CrystEngComm*, 2019, **21**, 1193.
20 P. C. Bunting, M. Atanasov, E. Damgaard-Møller, M. Perfetti, I. Crassee, M. Orlita, J. Overgaard, J. van Slageren, F. Neese and J. R. Long, *Science*, 2018, **362**, eaat7319.
21 V. Petříček, M. Dušek and L. Palatinus, *Z. Kristallogr. - Cryst. Mater.*, 2014, **229**, 345.
22 L. W. Schroeder and M. Mathew, *J. Solid State Chem.*, 1978, **26**, 383.
23 A. Orera, E. Kendrick, D. C. Apperley, V. M. Orera and P. R. Slater, *Dalton Trans.*, 2008, 5296.
24 S. M. J. Aubin, Z. Sun, L. Pardi, J. Krzystek, K. Folting, L.-C. Brunel, A. L. Rheingold, G. Christou and D. N. Hendrickson, *Inorg. Chem.*, 1999, **38**, 5329.
25 N. F. Chilton, R. P. Anderson, L. D. Turner, A. Soncini and K. S. Murray, *J. Comput. Chem.*, 2013, **34**, 1164.

Received: 29th June 2023; Com. 23/7207